Analysis and hydraulic improvement of a maturation pond using Computational Fluid Dynamics

Análisis y mejora hidráulica de un estanque de maduración mediante Dinámica de Fluidos Computacional

Luis Velázquez-Araque [ID]¹* Johan Chica [ID]²

¹Facultad de Ingeniería Química, Universidad de Guayaquil. Avenida Delta entre Avenida Kennedy. C. P. 090514. Guayaquil, Ecuador.
²Grupo de investigación Ambiente, Sociedad y Empresa (ASE), Universidad de Guayaquil. Avenida Delta entre Avenida Kennedy. C. P. 090514. Guayaquil, Ecuador.

ABSTRACT: Especially in small communities, little attention is paid to the hydraulic characteristics of wastewater treatment systems. Motivated by this problem, and using the ANSYS fluid dynamics software, the hydrodynamic evaluation of the residual water flow in a rural plant maturation pond was carried out. For the stationary modeling of the velocity and turbulence fields, the standard k-ε model was used; and for transient modeling of virtual tracer transport, the species transport model without chemical reaction was used. Subsequently, the analysis of the distribution of retention times was carried out, in order to obtain the flow patterns that govern the hydrodynamics of the pond. The results revealed the presence of hydraulic short circuits, stagnant zones, and recirculations, due to design deficiencies and operating conditions over the years. Given this situation, and by bibliographic recommendation, new modified geometries were proposed with longitudinal and transverse baffles at 70 and 90% in relation to the width and length of the pond. As a result, the hydraulic characteristics improved notably in all cases; however, the models configured at 90% achieved higher efficiency.

RESUMEN: Especialmente en pequeñas comunidades, se presta poca atención a las características hidráulicas de los sistemas de tratamientos de aguas residuales. Motivado en esta problemática, y empleando el paquete fluidodinámico de ANSYS, se realizó la evaluación hidrodinámica del flujo de agua residual en un estanque de maduración de una planta rural. Para la modelación estacionaria de los campos de velocidad y turbulencia, se empleó el modelo estándar k-ε; y para la modelación transitoria del transporte del trazador virtual, se utilizó el modelo de transporte de especies sin reacción química. Posteriormente, se elaboró el análisis de la distribución de los tiempos de retención, a fin de obtener los patrones de flujo que gobiernan la hidrodinámica de la laguna. Los resultados revelaron la presencia de cortocircuitos hidráulicos, zonas estancadas y recirculaciones; en consecuencia a deficiencias de diseño y condiciones operativas a través de los años. Ante esta situación, y por recomendación bibliográfica, se propusieron nuevas geometrías modificadas con deflectores longitudinales y transversales al 70 y 90% en relación al ancho y longitud del estanque. Producto de ello, las características hidráulicas mejoraron notablemente para todos los casos; sin embargo, los modelos configurados al 90% alcanzaron mayor eficiencia.

1. Introduction

Most communities in the world use stabilization ponds as a wastewater treatment method, almost always due to their attractive cost of operation. These lagoons are normally shallow excavations surrounded by earth slopes, with a

rectangular or square appearance [1].

The overall performance of a wastewater treatment system depends on the effectiveness of the biokinematic processes and the hydrodynamic performance of its lagoons. In order to evaluate this last aspect, tracer tests are usually used. However, these experiments have been insufficient for an absolute understanding of the hydrodynamics of the system. In addition, this practice is influenced by external factors not considered such as environmental or meteorological [2].

Computational fluid dynamics (CFD) offers the option of simulating the hydraulic behavior of one or several fluids in a specific system, thus avoiding resorting to experimentation or preventing unwanted events during the process [3].

Previous studies [4–8] have demonstrated the ability of CFD to predict the behavior of the flow inside a facility, which makes it possible to evaluate the hydraulics of the system and detect inefficiencies that affect the process. To increase the efficiency of wastewater treatment systems, and thereby favor the removal of contaminants, many of these studies have considered the incorporation of physical restrictions (baffles) [3].

Baffle design can vary significantly, but these structures are typically floating, waterproof, and anchored at the base. They generally allow variable water levels and have low installation costs [9]. The main functions performed by the baffles are to increase hydraulic retention time (HRT), reduce hydraulic short-circuiting, and provide a submerged surface that can encourage the growth of adjoining biomass [10]. However, in other cases [11, 12], baffles have not been found to increase HRT in stabilization ponds. Model studies have shown that certain flow conditions and baffle arrangements can inhibit mixing and reduce HRT. In particular, for very low flow velocities, baffles perpendicular to the direction of flow and ponds with a very high length-to-width ratio may have shorter HRTs as a result of the addition of hydraulic structures. Given this situation, other authors [13] emphasized the evaluation of the position and dimension of the baffles on the geometry of the pond.

Based on this analysis, two-dimensional studies were carried out on several modified proposals with baffles of a system of lagoons with variable length and width ratios. The results concluded that the configuration of baffles placed at 70 and 90% of the original size of the lagoon, obtained greater efficiency in pathogen removal [14].

Table 1 Dimensions of the maturation pond (MP

Location	Parameters	Dimensions (m)
Maturation pond	Height	1.26
	Width	76
	Length	310
Wall	Height	1.26
	Width	0.2
	Length	309

2. Materials and methods

2.1 Stabilization pond

The study was carried out at the wastewater treatment plant of the La Troncal canton, in charge of the drinking water and sewage company EMAPAT - EP, at coordinates: -2.407710910950- 09, -79.33729164878007.

Figure 1 presents the pond modeled in this study, whose dimensions are shown in Table 1. The inlet and outlet conduits are located at medium depth and parallel, separated by a concrete wall. Between the slopes and the dividing wall, the formation of openings due to climatic and operational conditions over the years was detected, which in turn were included in the geometry to analyze their influence on the HTR.

2.2 CFD modeling

According to [11], a two-dimensional modeling of stabilization ponds has been a good alternative to three-dimensional modeling, due to its simplicity and computational economy. In addition, other authors have indicated that when modeling very shallow depths, there is little variation in the velocity profile at depth [15, 16]. Therefore, a two-dimensional simulation of the MP shown in Figure 1 was performed using the ANSYS v.19.2 fluid dynamics software, with a second-order upwind numerical scheme and a SIMPLE pressure-momentum coupling.

Discretization of the domain

For this two-dimensional geometry, an unstructured mesh was created with the Quadrilateral Dominant mesh generation method, which prioritizes quadrilateral elements, and in conflicting areas, it is supplemented with triangular elements. As this study requires a greater level of detail in the analysis of the velocity and turbulence fields in the regions where these gradients are high, the incorporation of refinement was performed. A refinement of 0.01m was established for the inlet and outlet; the maximum element size was set at 3m, and for the edges of the walls and deflectors, three refinement sizes were

Figure 1 Diagram of the maturation pond La Troncal, Ecuador

tested: 1m for mesh 1 (M1), 0.5m for mesh 2 (M2) and 0.1m for the mesh 3 (M3).

Mesh independence analysis

For the mesh independence analysis, single-phase steady-state hydrodynamic modeling of M1, M2, and M3 was performed. Then, the velocity residuals were plotted, both in the X and Y direction.

Table 2 shows the results of the steady-state modeling configured for 1000 iterations, and Figures 2a and 2b show the X and Y velocity residuals. From these plots, it can be interpreted that M1 and M2 have a lot of similarities, coinciding at certain points after 700 iterations. However, the residuals of M1 are very distant from M3, with M2 being the one that best approximates its behavior with the least number of elements.

Therefore, based on the computational demand that this entails, the mesh size configuration selected as optimal for this study was M2, which contains 69453 quadrilateral elements and an orthogonal quality and obliquity of 0.9632 and 0.2023, respectively, resulting in a high-quality mesh.

Standard model $k - \varepsilon$

Since the flow regime is turbulent, for the stationary modeling of the velocity and turbulence fields, the standard k-ε model comprised by Equations 1 and 2 was used, which has been widely used in the modeling of stabilization ponds in CFD, with great success [2].

$$\frac{\partial}{\partial t}(\rho k) + \frac{\partial}{\partial x_i}(\rho k u_i) = \frac{\partial}{\partial x_j}\left[\left(\mu + \frac{\mu_t}{\sigma_k}\right)\frac{\partial k}{\partial x_j}\right] \quad (1)$$
$$+ G_k + G_b - \rho\varepsilon - Y_M + S_k$$

$$\frac{\partial}{\partial t}(\rho\varepsilon) + \frac{\partial}{\partial x_i}(\rho\varepsilon u_i) = \frac{\partial}{\partial x_j}\left[\left(\mu + \frac{\mu_t}{\sigma_\varepsilon}\right)\frac{\partial\varepsilon}{\partial x_j}\right] \quad (2)$$
$$+ C_{1\varepsilon}\frac{\varepsilon}{k}(G_k + C_{3\varepsilon}G_b) - C_{2\varepsilon}\rho\frac{\varepsilon^2}{k} + S_\varepsilon$$

In these equations, G_k represents the generation of turbulent kinetic energy due to mean velocity gradients. G_b is the generation of turbulent kinetic energy due to buoyancy. Y_M represents the contribution of the fluctuating dilatation in the compressible turbulence to the total dissipation rate. $C_{1\varepsilon}, C_{2\varepsilon} y C_{3\varepsilon}$ are constants. $\sigma_k y \sigma_\varepsilon$ are the Prandtl turbulence numbers for k and ε respectively.

The constants presented in advance have the following default values:

$$C_{1\varepsilon} = 1.44, \quad C_{2\varepsilon} = 1.92, \quad C_\mu = 0.09$$
$$\sigma_k = 1.0, \quad \sigma_\varepsilon = 1.3$$

Species transport model

There are two ways available to perform a virtual plotter test on CFD [17] . The first is to define a tracer (passive scalar) with the same properties as the study fluid; inject it at the input through the boundary conditions and monitor the concentration of this pseudo compound at the output. The second is to define solid particles that have the same density as the flowing fluid and a very small diameter, injecting a quantity large enough to obtain statistically significant results and observing the time it takes for each particle to leave the system. This study opted for the first alternative on the recommendation of a comparative study [18], which obtained a better fit for the experimental data. The equation for the conservation of mass for each chemical species i can be expressed in its mass fraction m_i, assuming that Fick's law holds [19].

$$\frac{\partial(\rho m_i)}{\partial t} + \nabla \cdot \left(\rho \vec{V} m_i\right) = \nabla \cdot (\rho D_i \nabla m_i) + R_i \quad (3)$$

averaging Equation 3 for the case of turbulent flow, it comes to Equation 4

$$\frac{\partial(\rho m_k)}{\partial t} + \frac{\partial}{\partial x_i}\left(\rho \vec{V}_i m_k\right) =$$
$$\frac{\partial}{\partial x_j}\left[\left(\rho D_k + \frac{\mu_t}{Sc_t}\right)\frac{\partial m_k}{\partial x_j}\right] + R_k \quad (4)$$

Boundary conditions

An inlet velocity profile was applied based on the nominal flow rate of the pumping equipment, the daily operation time, and the dimension of the inlet duct. The residence time distribution (RTD) analysis was performed by applying a transient simulation of the tracer as a scalar on the

Table 2 Residuals for stationary modeling of M1, M2, and M3

ITERATION	M1		M2		M3	
	Res. x-velocity	Res. y-velocity	Res. x-velocity	Res. y-velocity	Res. x-velocity	Res. y-velocity
100	1.23E-03	1.48E-03	1.42E-03	1.54E-03	2.01E-03	1.52E-03
200	3.83E-04	6.83E-04	5.84E-04	8.74E-04	4.03E-04	6.36E-04
300	1.43E-04	1.97E-04	2.68E-04	5.44E-04	2.42E-04	3.90E-04
400	6.64E-05	6.16E-05	1.37E-04	2.56E-04	1.83E-04	3.05E-04
500	3.40E-05	2.44E-05	8.17E-05	1.41E-04	1.38E-04	2.45E-04
600	2.05E-05	1.21E-05	4.27E-05	6.95E-05	1.18E-04	2.11E-04
700	1.43E-05	7.03E-06	2.37E-05	3.54E-05	1.02E-04	1.84E-04
800	1.03E-05	4.77E-06	1.98E-05	1.67E-05	9.68E-05	1.85E-04
900	7.65E-06	3.23E-06	6.25E-06	6.30E-06	1.24E-04	2.38E-04
1000	5.88E-06	2.35E-06	4.92E-06	2.68E-06	1.41E-04	2.85E-04
NODES	65840		75096		151566	
ELEMENTS	60834		69453		140770	

(a)   (b)
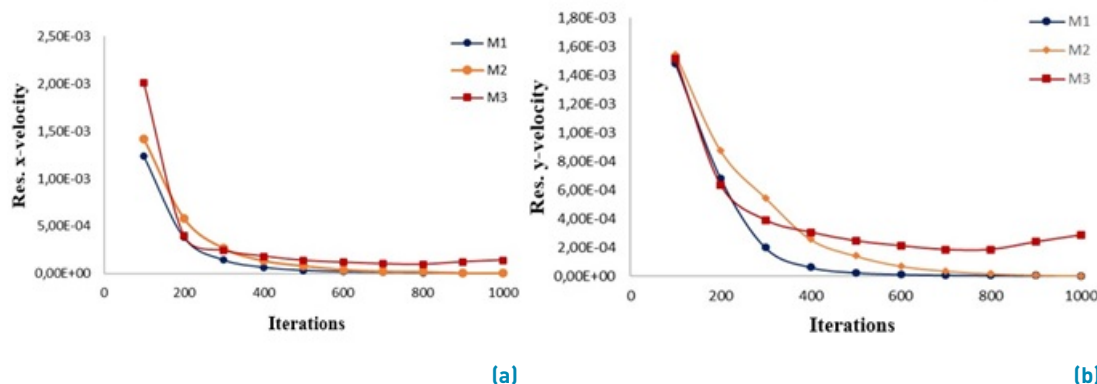
Figure 2 a) X-velocity Residuals Vs. Iterations for M1, M2, and M3 b) Y-velocity Residuals Vs. Iterationsfor M1, M2, and M3,

velocity and turbulent fields obtained from the stationary simulation. The properties of the tracer material were defined identically to those of the primary fluid. The tracer was injected at time t = 0 s for one- time step, giving a mass fraction of 1, and then reset to 0 s for the second and subsequent time steps. The RTD was obtained by generating a surface report of tracer concentration versus time at the pond outlet [20].

RTD Analysis

Being MP a large reactor, it is evident to believe that the elements that make up the fluid take different times to cross the entire control volume [21]. These deviations arise because of channeling, recirculation, or the creation of stagnant areas. In order to analyze these phenomena, the performance of the residence time curves was used. The hydraulic parameters from the RTD curves are shown in Table 3.

Pulse curve

The reading of the tracer concentration at the outlet of a reactor as a function of time is also known as the C_{pulse} curve, expressed in $kmol/m^3$ as shown in Figure 3a, where M represents the tracer concentration in kmol, v the fluid flow rate in m^3/s, $\bar{t}$ the mean residence time in days and V the volume in m^3. From the mass balance for the reactor, the area under the curve (Equation 5) and the mean of the curve (Equation 6) are obtained.

$$A = \int_0^\infty C dt \cong \sum_i C_i \Delta t_i = \frac{M}{V} \qquad (5)$$

$$6\bar{t} = \frac{\int_0^\infty t C dt}{\int_0^\infty C dt} \cong \frac{\sum_i t_i C_i \Delta t_i}{\sum_i C_i \Delta t_i} = \frac{V}{V} \qquad (6)$$
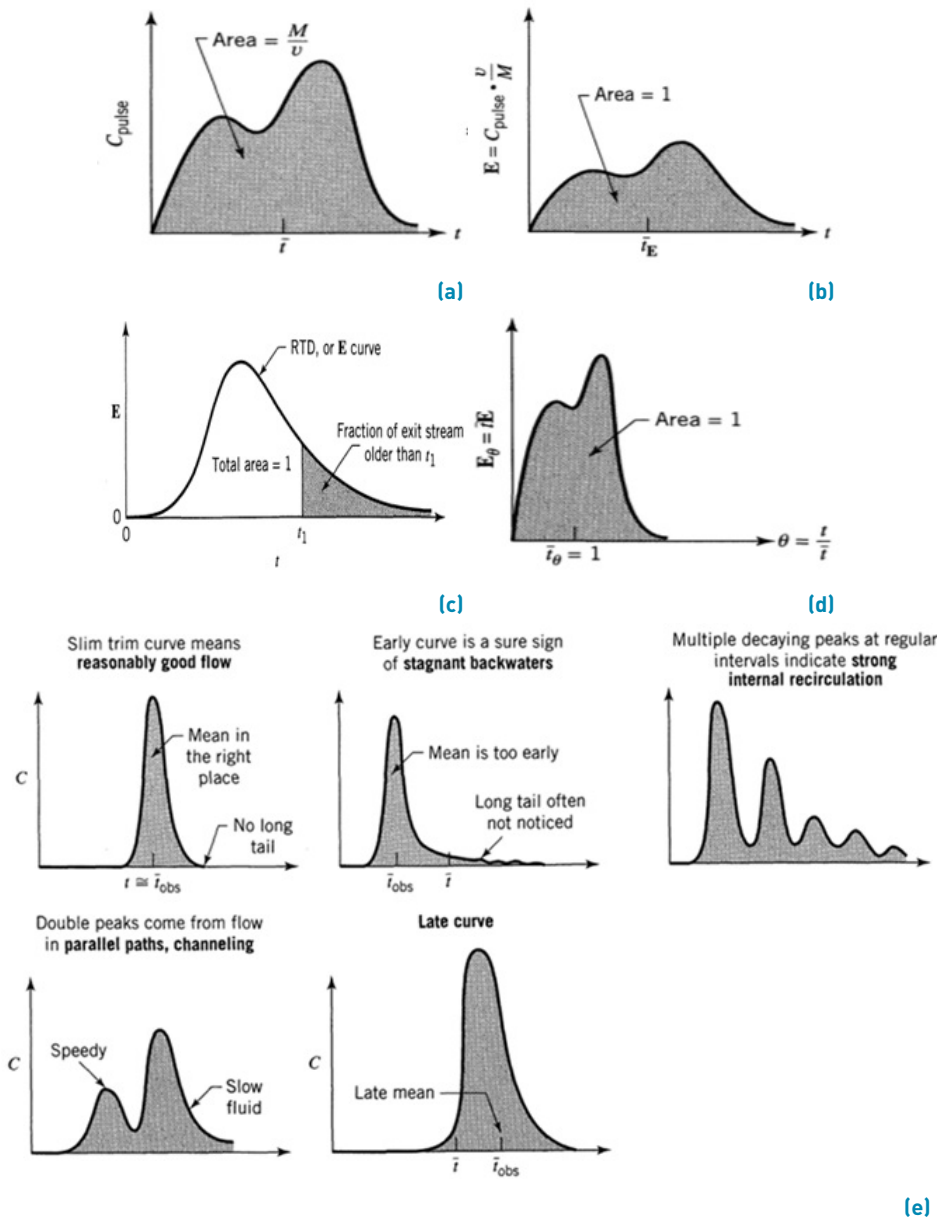
Figure 3 Residence time distribution curves. a) Pulse curve. b) E curve. c) Fluid fraction greater than t_1. d) Normalized E Curve. e) Hydraulic characteristics for plug-type flows

E Curve

To find the E curve from the C_{pulse} curve, only the concentration scale had to be changed, so that the area under the curve is unity. This is achieved by dividing the concentration readings by $\frac{M}{v}$, as shown in Figure 3b. Equation 7 represents the mathematical normalization of the RTD function, where the fraction of the fluid that meets a duration of time t inside the reactor, is given by the value of E(t)dt.

$$\int_0^\infty E(t)dt = 1 \qquad (7)$$

The fraction of the fluid that leaves the reactor with a duration less than t_1 is given by Equation 8.

$$\int_0^{t_1} E(t)dt \qquad (8)$$

Also, the fraction of the fluid with a duration greater than t_1 is obtained using Equation 9 and it is represented by the shaded area in Figure 3c.

$$\int_{t_1}^\infty E(t)dt = 1 - \int_0^{t_1} E(t)dt \qquad (9)$$

Normalized E curve

Finally, another RTD function was obtained, E_θ given by Equation 10. In this case, the time is measured as a function of the average residence time $\theta = \frac{t}{\bar{t}}$, as indicated in Figure 3d. For the characterization of the flow, dimensionless parameters of time θ and concentration were used E_θ, indicated in Figure 3e for plug-type flows [21].

$$E_\theta = \overline{tE} = \frac{V}{V} \cdot \frac{C_{pulse}}{\frac{M}{V}} = \frac{V}{M} \cdot C_{pulse} \qquad (10)$$

Quantitative analysis of residence time distribution

Once the DTR curves were obtained, following a statistical procedure, some of the parameters that define the hydraulic analysis of the pond were determined [12]. Dead zones are recognized as those sectors where the flow remains stagnant or circulates slowly. Active volume is the opposite definition of a dead zone. The short circuit index indicates an inversely proportional relationship to the strength of the short circuit; a positive change refers to a decrease in the strength of the short circuit, and therefore an increase in the hydraulic performance, where S = 1 represents an ideal plug flow behavior. And the Persson hydraulic efficiency, which describes the uniformity of the flow distribution within the pond, where 1 represents ideality and values close to zero, unsatisfactory behavior [21].

3. Results and discussion

3.1 Stationary modeling of the MP

The velocity contours obtained by CFD in Figure 4 show the phenomena caused by channeling, recirculation, or the creation of stagnant zones. The color palette of Figure 4a relates the flow velocity in each sector of the pond, while the lanes followed by the current can be seen in Figure 4b and the preferred directions of flow are indicated in Figure 4c by vector superposition.

3.2 Transient modeling of the MP

Injection and transport of the virtual tracer

The transient modeling was divided into two parts: tracer injection and tracer transport. The tracer was injected at time t = 0 s for a time step, giving a mass fraction of species equal to 1, and then the mass fraction was reset to 0 for the following time steps. For the tracer injection, the number of time steps was 10 with a size of 0.1 s and for the tracer transport, the number of time steps was 172800 with a size of 1 s (48 h) with 1 iteration per time step. These time step values ensure the independence of the results. The residence time distribution was obtained

by plotting the tracer concentration versus time at the pond outlet.

Figure 5a shows the virtual tracer concentration contours during one second of modeling. This process consists of the initial stage of the freezing method, or pulse experiment [18]. The subsequent stage indicated in Figures 5b-4e corresponds to the non-stationary modeling of the transport of the virtual tracer during a period of 4 days referred to the virtual environment, as a recovery criterion for most of the tracer.

The tracer distribution reveals the influence exerted by the opening in the wall next to the inlet. The flow recirculations in both blocks cover the entire length of the pond and make it impossible for the tracer to progress. As a result, there is a tracer available in low concentrations, but distributed over most of the pond, and especially over the return sector.

3.3 Analysis of RTD curves

Figure 6a reports the shape adopted by the pulse curve, which revealed the reading of high tracer concentrations during the initial modeling stage, due to the presence of hydraulic short circuits; and between days 0.5 and 4, a notable reduction in the concentration read at the outlet of the unit was observed.

By converting the area under the curve to unity, it was required to know the fraction of fluid that leaves the pond during the stage that gives rise to the formation of the crest of the curve presented in Figure 6b. The reference duration was 10 hours. And under this criterion, it was determined that 34% of the fluid leaves the pond.

Figure 6c plots the location of the normalized retention time on the tail of the normalized E-curve; this behavior revealed the presence of stagnant zones and recirculation problems.

3.4 Quantitative analysis of RTD curves

The first parameter found in Table 4 was the mean retention time, located in curve 5a on the elongated area of the tail. This phenomenon supposes the presence of stagnant zones where the CFD-simulated tracer slowly diffuses out of the MP [20].

The short-circuit index obtained reveals the presence of short-circuits, specifically in the inlet sector since S = 1 represents an ideal plug flow behavior, without the presence of short-circuits [11].

Table 3 Hydraulic parameters from the RTD curves

$$V_d = \left(1 - \frac{\bar{t}}{\tau}\right) \cdot 100\%$$

V_d = Dead volume (%)
$\bar{t}$ = Mean retention time (days)
τ = Theoretical retention time (days), a measure of the average length of time that a soluble compound remains in the MP.
V_act = Active volume (%)

$$V_{act} = \left(\frac{\bar{t} \cdot V}{Vol}\right) \cdot 100\%$$

V = Input flow rate $\left(m^3/d\right)$
Vol = Volume of the pond $\left(m^3\right)$

$$S = \frac{t_{16}}{\tau}$$

S = short circuit rating
$t_1 6$ = Time where 16% of the tracer has traversed the outlet (days)

$$\lambda_p = \frac{t_p}{\tau}$$

λ_p = Persson Hydraulic Efficiency
t_p = Time that records the highest concentration of tracer (days)

(a) (b) (c)
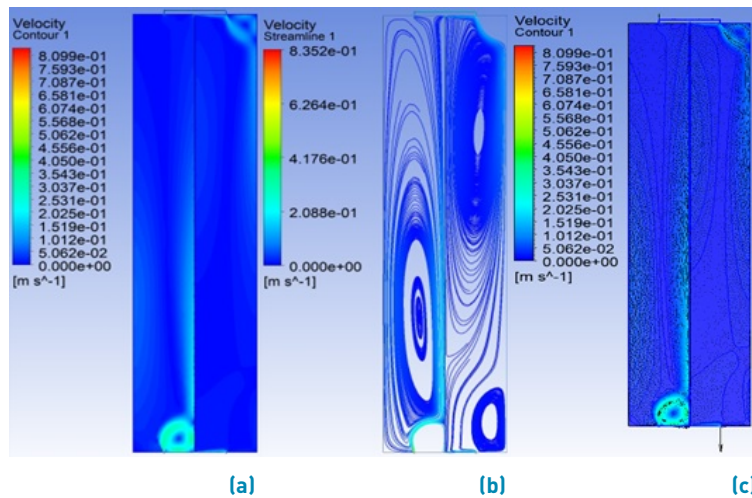
Figure 4 Contours generated from the stationary modeling for MP. a) Velocity contours. b) Velocity streamlines. c) Velocity Vectors plus contours

(a) (b) (c) (d) (e)
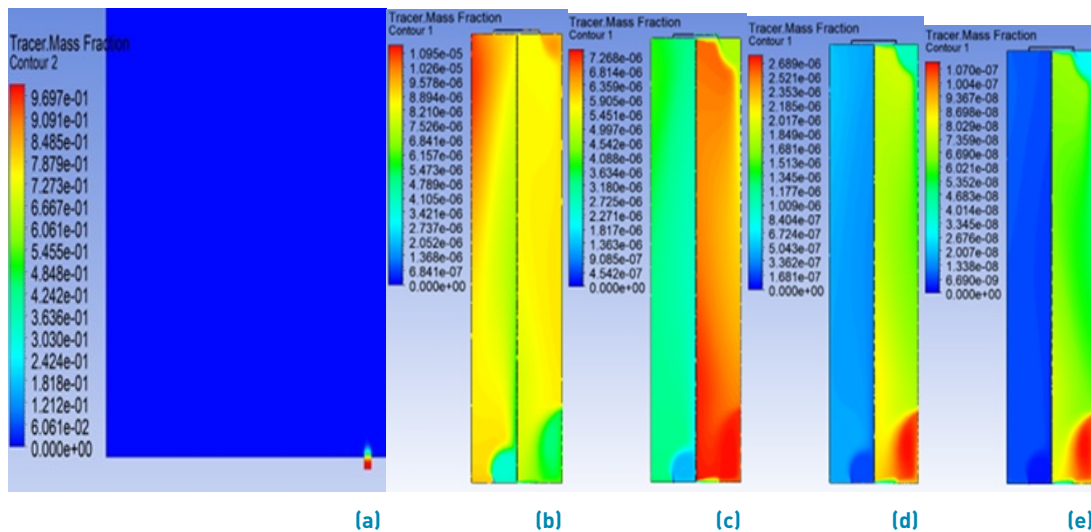
Figure 5 Tracer concentration across the pond as a function of modeling time. a) Virtual Tracer Injection b) After 12 hours of simulation. c) After 1 day of simulation d) After 2 days of simulation. e) After 4 days of simulation

The high percentage of dead volume affects the importance of the location of the inlet and outlet conduit, as well as

(a)

(b)

(c)
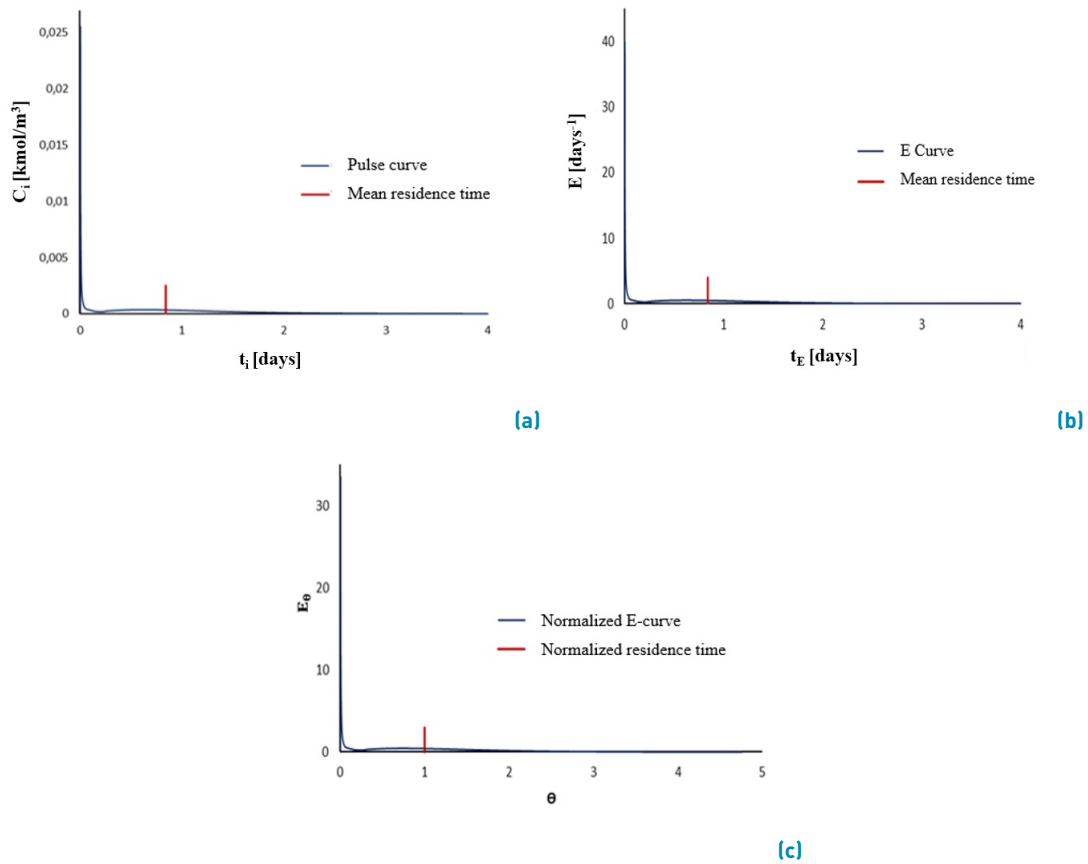
Figure 6 Contours generated from the stationary modeling for MP. a) Velocity contours. b) Velocity streamlines. c) Velocity Vectors plus contours

Table 4 Hydraulic parameters from RTD analysis

Code	Mean retention time (h)	Short circuit rating	Dead volume (%)	Active volume (%)	Hydraulic efficiency according to Persson
MP	0.8411	0.0023	22.6767	77.3232	0.0037

the dispersion dependent on the length-width ratio of the pond [22–24].

Finally, the hydraulic efficiency (λp) with a value that tends to 0, indicated a poor performance [25], as a result of the parallel relationship between the inlet and outlet of the pond.

3.5 Optimization proposals

Having verified the hydraulic inefficiency of the MP and following the recommendation of previous studies carried out in stabilization pond systems, six modified geometric proposals were built with baffles configured at 70% [26], and 90% [14] in relation to the length and width of the pond. In order to present a possible solution to carry out in practice, the arrangement of the inlet and outlet ducts was preserved. The opening between the lower slope and the

dividing wall was closed, and the latter was transformed into a longitudinal deflector, as can be seen in Table 5.

3.6 Stationary and transient modeling for the modified proposals

Table 6 shows the flow streamlines obtained in the stationary modeling for the modified proposals with baffles, and the tracer concentration contours during the non-stationary modeling under the same MP modeling criteria. A mesh independence analysis for all these configurations (P1 to P6) was also carried out.

The geometrically modified proposals, except for P3, revealed the influence of the incorporation of deflectors on the successive transport of the virtual tracer; in addition,

Table 5 Proposed geometries for the MP

Code	Geometry	Number of baffles	Aspect ratio 70%	Aspect ratio 90%
P1		7	✓	
P2		10	✓	
P3		13	✓	
P4		7		✓
P5		10		✓
P6		13		✓
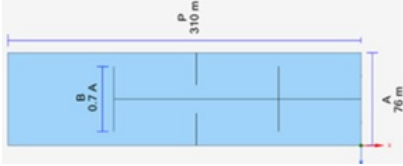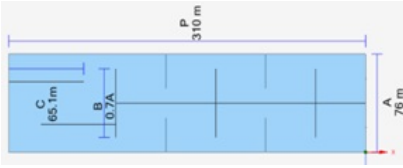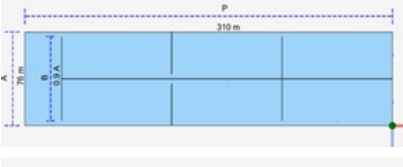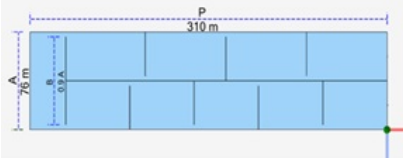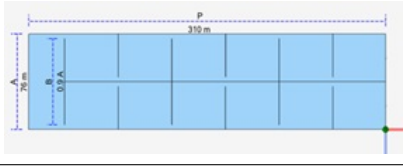
the hydraulic benefits of reducing recirculation to sectors can be visualized.

P3 indicates the formation of a stagnant zone between the upper left corner of the pond and the first longitudinal baffle. The placement of the longitudinal baffles at very short distances did not improve the progressive transport of the tracer for this case study.

3.7 RTD Analysis for modified proposals

Figure 7a shows the comparison of the surface profiles generated from the non-stationary modeling of the MP and the modified proposals. Two important aspects to highlight are the shape of the tail of the curve relevant to MP and the oscillations during the initial stage of tracer reading in P1. Previous investigations [15, 27] indicate this behavior because of the presence of hydraulic short-circuits and recirculations, respectively. In this study, it is specifically reflected because of the opening in the wall in the case of MP, and the wide distance between the deflectors that make up P1.

As indicated in the RTD analysis of MP, a useful characteristic of the E curve is to define the area under the curve as unity; this function allows analyzing the fraction

Table 6 Contours of the stationary and transient modeling for the modified proposals

Code	Velocity streamlines	Virtual tracer transport		
		12 hours	2 days	4 days
P1				
P2				
P3				
P4				
P5				
P6				

(a)

(b)

(c)
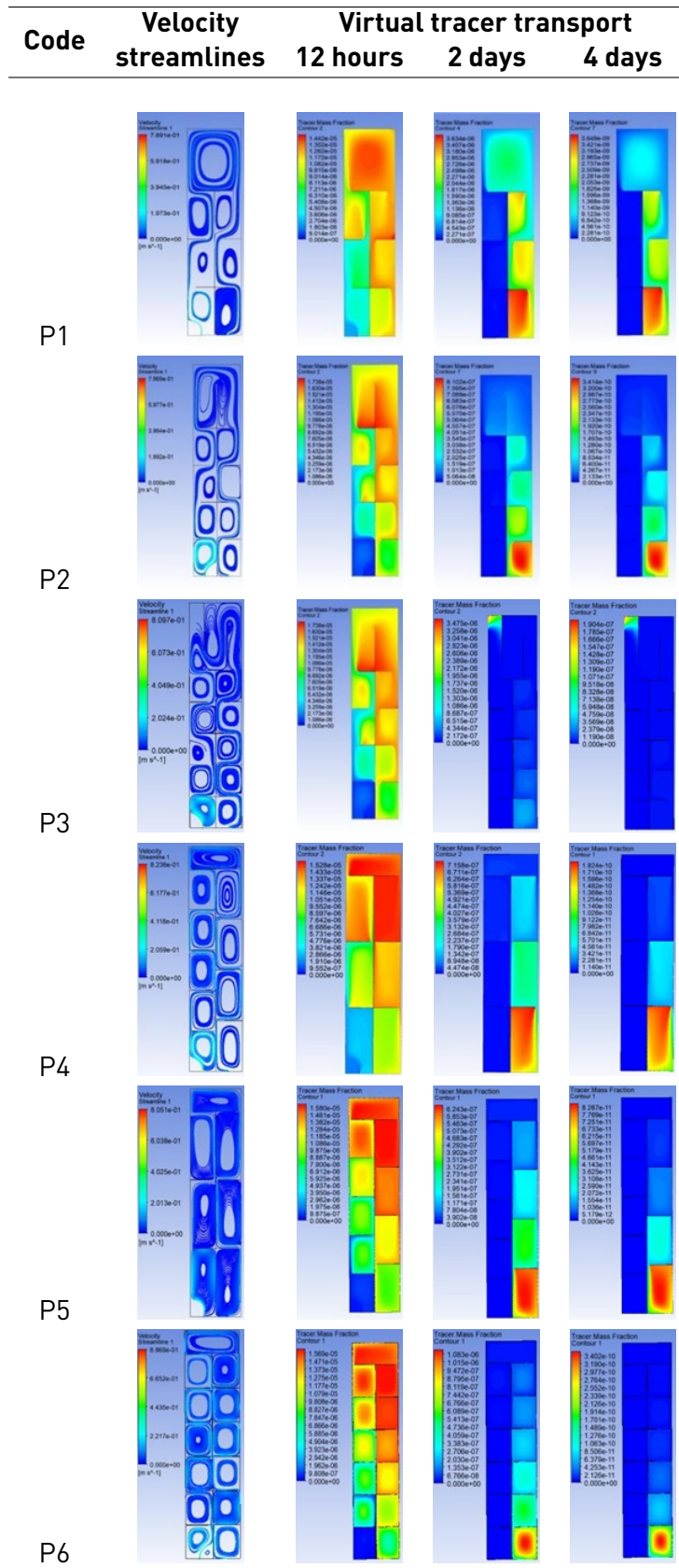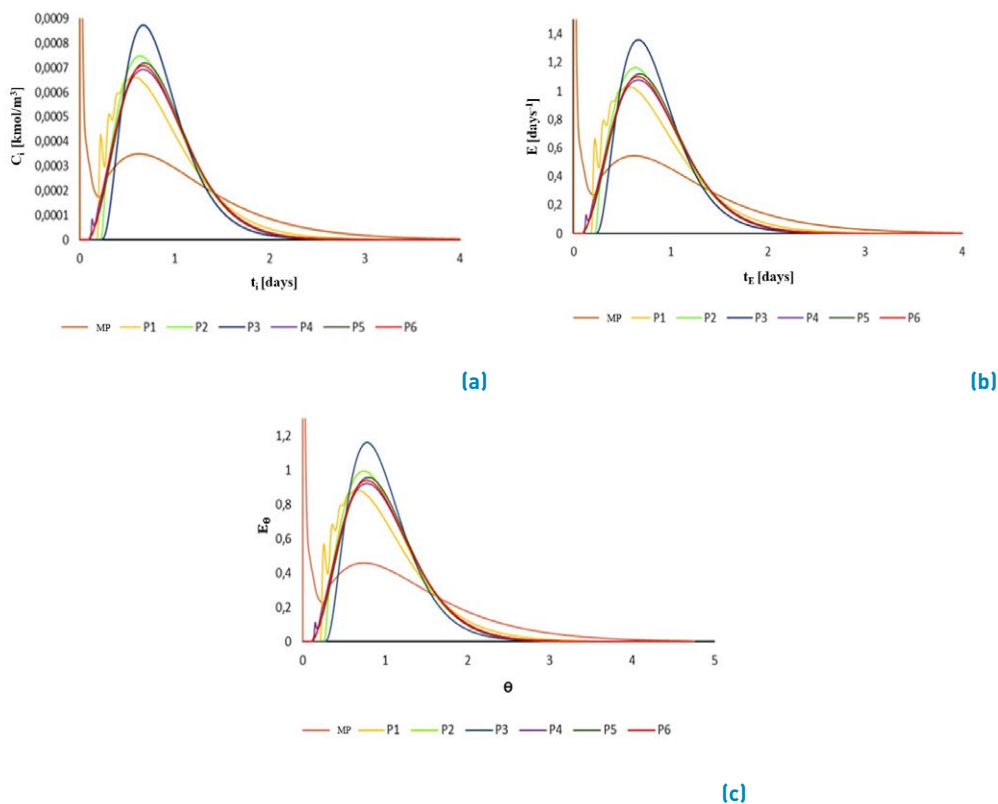
Figure 7 Comparison between the RTD curves of the MP and the modified proposals. a) Pulse curve. b) E curves. c) Normalized E curves

of fluid that remains or leaves the reactor at the requested instant of time. For the cases of the modified proposals in Figure 7b, the reference age was the same as for MP. The results showed that fluid fractions of approximately 11% left the ponds P4, P5, and P6 in a common way, while the percentage of fluid dislodged for P1 was close to 15%. For their part, P2 and P3 reported dislodged fluid fractions equal to 5% and 9%, respectively, these being the most favorable results in terms of fluid retention during the initial test stage.

Through hydraulic characterization for plug-type flows [21] the phenomena immersed in the pond, described in Figure 3e, were predicted. Among the modified proposals, P2 and P3 better represent the behavior of a reactor that does not present anomalies, due to the location of the normalized mean retention time in relation to the crest of the curves. The formation of stagnant zones and recirculation problems become more noticeable for MP compared to the modified proposals and the influence of the distance between the baffles for P1 during the initial tracer reading is reiterated (Figure 7c).

3.8 Quantitative analysis of the RTD curves for the modified proposals

The results shown in Table 7 show the similarity between the mean retention times of the proposals and MP, due to the tracer retention capacity on stagnant zones and elongated recirculations. Among the proposals with 70% baffles, P3 has the best short-circuit index; and among the proposals with 90%, P4 presents the best index. The MP index is 92 times lower than P3, being the option that best approximates the ideal behavior plug flow.

Approximately 1% of the active volume was recovered by the inclusion of baffles. As mentioned above, the possibility of reducing stagnant areas depends essentially on the position and the number of inlets and outlets, which were preserved according to their origin in order to present a real optimization alternative to the treatment system.

The difference between the hydraulic efficiency of MP and the modified proposals shows the importance of closing the opening next to the inlet. Among the proposed cases, P5 achieved the best result, and among the configurations at 70%, only proposal P3 presented a result of interest. The efficiency of the P4 model has an intermediate value

Table 7 Hydraulic parameters from RTD analysis

Parameter	P1	P2	P3	P4	P5	P6
Mean retention time (h)	0.8558	0.8552	0.8533	0.8551	0.8547	0.8539
Short circuit rating	0.1639	0.1937	0.2129	0.0996	0.0939	0.0876
Dead volume (%)	21.282	21.256	21.3581	21.2762	21.2462	21.2511
Active volume (%)	78.7172	78.7431	78.6418	78.7237	78.7537	78.7488
Persson Hydraulic Efficiency	0.5060	0.5860	0.6164	0.6155	0.6295	0.6146

between P3 and P5; however, its construction volume is lower and, therefore, a cheaper option, due to its number of baffles.

4. Conclusions

The modified proposals with baffles at 90% in relation to length and width reported more favorable results in this study. Among the proposals modified at 70%, only P3 reported good results in terms of short circuit index and percentage of fluid retained during the first hours of simulation; however, the values obtained regarding the mean hydraulic retention time and active volume were unfavorable, compared to the proposals at 90%. Additionally, P3 has a greater construction volume due to the number of deflectors (13), which translates into a configuration that is not recommended in terms of costs. In relation to this last aspect, P4 is more viable than P5. As obtained in the analysis of the E curves, the percentage of fluid retained during the first hours of simulation for P4 and P5 were similar; this is not the case for the mean hydraulic retention time and short-circuit index, where the proposal with 7 baffles reported more favorable results. Finally, in terms of hydraulic efficiency, P5 stands out with a higher percentage, but not excessive compared to P4. Therefore, P4 was considered the optimal configuration among the options covered for this case study.

5. Declaration of competing interest

We declare that we have no significant competitive interests, such as financial, professional, or personal interests that interfere with the complete and objective presentation of the work described in this document.

6. Acknowledgments

7. Funding

8. Author contributions

Luis Velazquez-Araque conceived and designed the study, performed data analysis and interpretation. Johan Chica collected the data, performed the simulations, and wrote the manuscript.

9. Data availability statement

The data that support the findings of this study are openly available in Mendeley Data at https://data.mendeley.com/datasets/v4sdygvyvs/1

References

[1] J. A. Rodríguez-Serrano, "Tratamiento de aguas residuales en pequeñas comunidades," B. A. thesis, Ingeniería, Universidad de Sonora, Hermosillo, México, 2008.

[2] A. Alvarado, S. Vedantam, G. Durazno, and I. Nopens, "Evaluación hidráulica de estanques de estabilización de residuos: comparación de simulaciones de dinámica de fluidos computacional con datos de trazadores," *Maskana*, vol. 2, no. 1, Jun. 24, 2011. [Online]. Available: https://doi.org/10.18537/mskn.02.01.05

[3] F. Cortés-Martínez, A. Treviño-Cansino, M. A. Alcorta-García, A. Sáenz-López, and J. L. González-Barrios, "Optimización en el diseño de lagunas de estabilización con programación no lineal," *Tecnología y Ciencias del Agua*, vol. 6, no. 2, Mar-Apr, 2015. [Online]. Available: https://www.scielo.org.mx/pdf/tca/v6n2/v6n2a6.pdf

[4] A. V. V. Castañeda, "Evaluación, mejoramiento y optimización hidráulica del sistema de lagunas de estabilización de san josé aplicando modelos cfd – lambayeque, 2017," B. A. thesis, Escual de Ingeniería Civil Ambiental, Universidad Católica Santo Torivio de Mogrovejo, Chiclayo, Perú, 2019.

[5] G. Aldana and N. Bracho, "Simulation and prediction of hydrodynamic performance at university of zulia's wastewater stabilization ponds using a 3d-computational fluid dynamic (cfd) model," *Revista Técnica de la Facultad de Ingeniería Universidad del Zulia*, vol. 8, no. 1, Jan. 2005. [Online]. Available: https://www.scielo.org.mx/pdf/tca/v6n2/v6n2a6.pdf

[6] A. M. Zapata-Rivera, J. Ducoste, M. R. Peña, and M. Portapila, "Computational fluid dynamics simulation of suspended solids transport in a secondary facultative lagoon used for wastewater

treatment," *Water*, vol. 13, no. 17, Aug. 23, 2021. [Online]. Available: https://doi.org/10.3390/w13172356

[7] A. Alvarado, E. Sánchez, G. Durazno, M. Vesvikar, and I. Nopens, "Cfd analysis of sludge accumulation and hydraulic performance of a waste stabilization pond," *Water Science & Technology*, vol. 66, no. 11, Dec. 2012. [Online]. Available: https://doi.org/10.2166/wst.2012.450

[8] V. Andrade-Rosero, "Estudio de la hidrodinámica y eliminación de coliformes fecales en la laguna de maduración de la depuradora de aguas residuales de la ciudad de portoviejo, ecuador, mediante modelos cfd con openfoam," MSc. thesis, Ingeniería Hidraúlica y Medio Ambiente, Universidad Politécnica de Valencia, Portoviejo, Ecuador, 2021.

[9] F. R. Spellman and J. E. Drinan, *Wastewater Stabilization Ponds*, 1st ed. Boca Ratón, EU: C. R. C Press, 2014.

[10] S. B. Nielson, E. J. Middlebrooks, and D. B. Porcella, "Effects of baffles on the p ects of baffles on the performance of aner formance of anerobic waste stabilization ponds," The Utah Water Research Laboratory, Utah, EU, Tech. Rep. Paper 172, Jan. 1973.

[11] L. X. Coggins, J. Sounness, L. Zheng, M. Ghisalberti, and A. Ghadouani, "Impact of hydrodynamic reconfiguration with baffles on treatment performance in waste stabilisation ponds: A full-scale experiment," *Water*, vol. 10, no. 2, Jan. 23, 2018. [Online]. Available: https://doi.org/10.3390/w10020109

[12] S. Li, J. Nan, and F. Gao, "Hydraulic characteristics and performance modeling of a modified anaerobic baffled reactor (mabr)," *Chemical Engineering Journal*, vol. 284, Jan. 15, 2016. [Online]. Available: https://doi.org/10.1016/j.cej.2015.08.129

[13] A. N. Shilton and D. D. Mara, "Cfd (computational fluid dynamics) modelling of baffles for optimizing tropical waste stabilization pond systems," *Water Science & Technology*, vol. 51, no. 12, Jun. 2005. [Online]. Available: https://doi.org/10.2166/wst.2005.0438

[14] H. Abbas, R. Nasr, and H. Seif, "Study of waste stabilization pond geometry for the wastewater treatment efficiency," *Ecological Engineering*, vol. 28, no. 1, Nov. 2006. [Online]. Available: https://doi.org/10.1016/j.ecoleng.2006.03.008

[15] T. M. Teshome, "Computational fluid dynamics application to optimize and evaluate the performance of high rate algal pond system," PhD. thesis, Université de Strasbourg, Strasbourg, France, 2020.

[16] F. Sánchez-Fernández, "Análisis y mejora de la fluidodinámica en estaciones depuradoras de aguas residuales," PhD. thesis, Escuela Internacional de Doctorado, Universidad Politécnica de Cartagena, Cartagena, Colombia, 2019.

[17] J. M. Fernández-Oro, *Técnicas numéricas en ingeniería de fluidos : introducción a la dinámica de fluidos computacional (CFD) por el método de volúmenes finitos*, 1st ed. Barcelona, ES: Reverté, Barcelona, 2012.

[18] S. Vedantam, J. B. Joshi, and S. B. Koganti, "Cfd simulation of rtd and mixing in the annular region of a taylor–couette contactor," *Industrial & Engineering Chemistry Research*, vol. 45, no. 18, Aug. 03, 2006. [Online]. Available: https://doi.org/10.1021/ie050825n

[19] O. Levenspiel, *Chemical Reaction Engineering*, 3rd ed. Oregon, EU: Wiley, 1998.

[20] D. O. Olukanni and J. J. Ducoste, "Optimization of waste stabilization pond design for developing nations using computational fluid dynamics," *Ecological Engineering*, vol. 37, no. 11, Nov. 2011. [Online]. Available: https://doi.org/10.1016/j.ecoleng.2011.06.003

[21] J. Persson, "The hydraulic performance of ponds of various layouts," *Urban Water*, vol. 2, no. 3, Sep. 2000. [Online]. Available: https://doi.org/10.1016/S1462-0758(00)00059-5

[22] A. Shilton, "Potential application of computational fluid dynamics to pond design," *Water Science & Technology*, vol. 42, no. 10, Nov. 01, 2000. [Online]. Available: https://doi.org/10.2166/wst.2000.0673

[23] A. Shilton and J. Harrison, "Integration of coliform decay within a cfd (computational fluid dynamic) model of a waste stabilisation pond," *Water Science & Technology*, vol. 48, no. 2, Jul. 01, 2003. [Online]. Available: https://doi.org/10.2166/wst.2003.0122

[24] J. García, J. Chiva, P. Aguirre, E. Álvarez, J. P. Sierra, and *et al.*, "Hydraulic behaviour of horizontal subsurface flow constructed wetlands with different aspect ratio and granular medium size," *Ecological Engineering*, vol. 23, no. 3, Nov. 01, 2004. [Online]. Available: https://doi.org/10.1016/j.ecoleng.2004.09.002

[25] A. Shilton and J. Harrison, "Development of guidelines for improved hydraulic design of waste stabilisation ponds," *Water Science & Technology*, vol. 48, no. 2, Jul. 01, 2003. [Online]. Available: https://doi.org/10.2166/wst.2003.0114

[26] D. Burgos-Flores, "Modelación del comportamiento hidráulico de unidades de tratamiento de agua y su validación en un proceso de sedimentación," PhD. thesis, Centro de Investigación en Materiales Avanzados, Chihuahua, México, 2008.

[27] C. A. Caro-Camargo and J. A. Bayona-Romero, "Hydro-dynamic modeling for identification of flooding zones in the city of tunja," *Revista Facultad de Ingeniería, Universidad de Antioquia*, no. 88, Sep. 18, 2018. [Online]. Available: https://doi.org/10.17533/udea.redin.n88a05